Supplementary information of Laser-induced ultrafast spin-transfer processes in non-linear zigzag carbon chain systems

Mohamed Barhoumi,[1, *] Jing Liu,[2, †] Georgios Lefkidis,[1, ‡] and Wolfgang Hübner[1, §]

[1] *Department of Physics, Rheinland-Pfälzische Technische Universität Kaiserslautern (RPTU) Kaiserslautern-Landau, P.O. Box 3049, 67653 Kaiserslautern, Germany*
[2] *Institute of Theoretical Chemistry, Ulm University, 89081 Ulm, Germany*
(Dated: August 1, 2023)

I. THEORY AND METHODS

A. CCSD and EOM-CCSD methods

We employ the coupled-cluster (CC) method to compute the many-body wave function of the ground state:

$$|\Psi\rangle = e^{\hat{T}}|\Phi_0\rangle. \tag{1}$$

The ground state wave function obtained from the Hartree-Fock method is $|\Phi_0\rangle$ (reference state of the CC calculations). The cluster operator is represented by $\hat{T}$.

$$\hat{T} = \hat{T}_1 + \hat{T}_2 + \hat{T}_3 + ...\hat{T}_N. \tag{2}$$

$\hat{T}_1$, $\hat{T}_2$, $\hat{T}_3$, etc, collectively designate single, double, and triple excitation operators, respectively. Those operators can be written in second quantization, e.g., $\hat{T}_1$ and $\hat{T}_2$ are

$$\hat{T}_1 = \sum_a \sum_r t_a^r \hat{a}_r^+ \hat{a}_a. \tag{3}$$

$$\hat{T}_2 = \frac{1}{4} \sum_{a,b} \sum_{r,s} t_{ab}^{rs} \hat{a}_r^+ \hat{a}_s^+ \hat{a}_b \hat{a}_a. \tag{4}$$

t_a^r and t_{ab}^{rs} are the expansion coefficients of the corresponding operators and are called amplitudes. The subscripts a, b, and the superscripts r, and s denote the index of occupied and unoccupied orbitals, respectively. $\hat{a}^+$ and $\hat{a}$ are creation and annihilation operators, respectively.

The correlated excited states of a system can be computed employing the equation of motion coupled-cluster method (EOM-CCSD). We can create several multi-configurational wave functions using this technique as well as a single reference formalism. The CCSD (reference) state serves as the foundation for the EOM-CCSD excited states. The general formalism for the excited state wave function is

$$|\Psi_e\rangle = \hat{R}|CC\rangle = \hat{R}e^{\hat{T}}|\Phi_0\rangle. \tag{5}$$

A linear excitation operator is described by $\hat{R}$ and referred to as an EOM-CCSD operator. For the case of EOM-CCSD, both $\hat{T}$ and $\hat{R}$ are truncated at single and double excitations.

B. SOC Hamiltonian and Time-Dependent Perturbation Theory

As we mentioned in the main text, SOC and a static external magnetic field are required in our study. SOC and magnetic field are perturbatively added

$$\hat{H}^{\text{SOC+B}} = \sum_{i=1}^n \frac{Z_a^{\text{eff}}}{2c^2 R_i^3} \hat{\mathbf{L}} \cdot \hat{\mathbf{S}} + \sum_{i=1}^n \mu_L \hat{\mathbf{L}} \cdot \mathbf{B}_{\text{stat}}$$
$$+ \sum_{i=1}^n \mu_{\mathbf{S}} \hat{\mathbf{S}} \cdot \mathbf{B}_{\text{stat}}. \tag{6}$$

---

* mbarhou@rptu.de
† jing-1.liu@uni-ulm.de
‡ lefkidis@rptu.de
§ huebner@rptu.de

$\hat{\mathbf{S}}$ and $\hat{\mathbf{L}}$ are the spin and the orbital angular momentum operators, respectively. The position vector of the i-th electron, relativistic effective nuclear charges of the a-th atom, and speed of light are represented by R_i^3, Z_a^{eff}, and c respectively. $\mu_{\mathbf{L}}$ and $\mu_{\mathbf{S}}$ describe the gyromagnetic ratios. The time-dependent interaction between the laser pulse and the many-body wave functions is represented by

$$\hat{H}'(t) = \hat{\mathbf{D}} \cdot \mathbf{E}_{\text{laser}}(t). \tag{7}$$

The electric dipole-transition operator and the time-dependent electric field of the laser pulse are represented by $\hat{\mathbf{D}}$ and $\mathbf{E}_{\text{laser}}(\mathbf{t})$, respectively. The propagation of the many-body wave function is performed within the interaction picture:

$$\frac{\partial c_n(t)}{\partial t} = \frac{-i}{\hbar} \sum_k \langle \Phi_n | \hat{H}'(t) | \Phi_k \rangle c_k(t) e^{-\frac{i}{\hbar}(E_k - E_n)t}. \tag{8}$$

The initial and final states are symbolized by n and k. Φ, obtained from CCSD and EOM-CCSD calculations and modified with the influence of SOC and B, is the wave function of the many-body states. E and c describe the population and energy of the many-body states, respectively. The aforementioned differential equations in Eqs. (8) are quantitatively determined using the Cash-Karp adaptive-step-size control and an embedded fifth-order Runge-Kutta technique. We employ our algorithm program to optimize the parameters of the laser pulse and efficiently reach the desired spin process.

We move beyond one laser pulse by applying double laser pulses to induce spin-down (or spin-up) spin transfer processes in the non-linear zigzag carbon chain structures to which two Ni magnetic centers are attached. The equation (8) becomes:

$$\frac{\partial c_n(t)}{\partial t} = \frac{-i}{\hbar} \sum_k \langle \Phi_n | \hat{H}_{\text{int}1}(t) + \hat{H}_{\text{int}2(t)}(t + \delta t) | \Phi_k \rangle c_k(t) \times \exp(-i(E_k - E_n)t/\hbar), \tag{9}$$

The interaction Hamiltonians of the initial and target laser pulses are $\hat{H}_{\text{int}1}(t)$ and $\hat{H}_{\text{int}2(t)}$, respectively. The time delay between two laser pulses is represented by δt.

C. Concept of Λ process

The fundamental purpose of the Λ process is to transfer the electronic population from the initial state $|n\rangle$ to the final state $|m\rangle$ via intermediate state $|l\rangle$ (see Fig. 1). We consider that the spin-dynamics Λ process is successfully induced under a laser pulse if its fidelity is higher than 70%. A spin-transfer process can occur if the spin densities of states $|n\rangle$ and $|m\rangle$ are localized on various magnetic centers. The process is known as a spin-flip process if the spin density is localized on the same atom with the initial and goal states having opposite spin orientations. The $|l\rangle$ intermediate states must be spin-mixed for the spin-flip process.
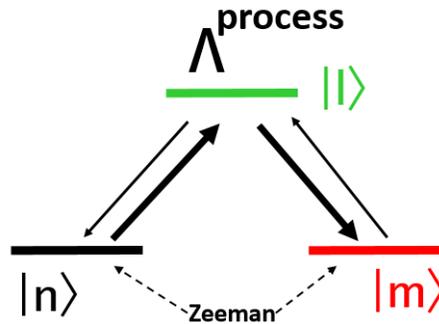

FIG. 1. Our main idea is to establish a laser-induced population shift from one state to another via an intermediate state. An excitation from the starting state to an electronically higher-lying intermediate state is followed by a deexcitation from the intermediate state to the final state in such a transition scenario. This process is called the Λ process. It is possible to accomplish a spin-transfer process if the spin densities of states $|n\rangle$ and $|m\rangle$ are localized on various magnetic centers. A spin-flip scenario can be accomplished if the spin densities of $|n\rangle$ and $|m\rangle$ are localized on the same atom but have different spin orientations ($\alpha \uparrow$ and $\beta \downarrow$). A Zeeman splitting is induced under the application of the magnetic field. Spin-mixing is required for the $|l\rangle$ intermediate states of a spin-flip process.

II. SPIN DENSITY DISTRIBUTION AND SPIN DYNAMICS PROCESSES ON $NI_2@C_{32}H_{32}$ AND $NI_2@C_{36}H_{36}$

In Table I, we show the spin density distribution, energies, and expectation values of the spin angular momentum elements for the spin-flip and spin-transfer scenarios on non-linear zigzag carbon chain structure $Ni_2@C_{32}H_{32}$ for the appropriate many-body states before and after inclusion spin-orbit-coupling and the magnetic field.

TABLE I: Spin density, energies, and expectation values of the spin angular momentum elements for the spin-flip and spin-transfer scenarios on non-linear zigzag carbon chain structure $Ni_2@C_{32}H_{32}$ for the appropriate many-body states before and after inclusion spin-orbit-coupling and the magnetic field. The sign of $\langle S_x \rangle$, $\langle S_y \rangle$, and $\langle S_z \rangle$ signifies the spin direction: the positive and negative values are spin-up $\alpha \uparrow$ and spin-down $\beta \downarrow$, respectively.

Method	States	Spin density before SOC and B Ni1	Ni2	E (eV)	$\langle S_x \rangle$	$\langle S_y \rangle$	$\langle S_z \rangle$	Energy, spins directions and spin density after SOC and B Ni1	Ni2
EOM-CCSD	$|77\rangle$	0.000	0.000	3.509730	0.000	0.000	0.000	0.000	0.000
	$|76\rangle$	0.006	1.050	3.371310	0.000	0.000	1.000	0.992	0.062
	$|75\rangle$	0.000	0.000	3.371260	0.000	0.000	0.000	0.000	0.000
	$|74\rangle$	-0.006	-1.050	3.371200	0.000	0.000	-1.000	-0.992	-0.062
	$|73\rangle$	0.000	0.000	3.239990	0.000	0.000	1.000	0.069	0.569
	$|72\rangle$	0.000	0.000	3.239930	0.000	0.000	0.000	0.000	0.000
	$|71\rangle$	1.016	0.002	3.239880	0.000	0.000	-1.000	-0.069	-0.569
	$|70\rangle$	0.000	0.000	3.170420	0.000	0.000	1.000	-0.013	1.009
	$|69\rangle$	-1.016	-0.002	3.170370	0.000	0.000	0.000	0.000	0.000
	$|68\rangle$	0.011	1.021	3.170320	0.000	0.000	-1.000	0.013	-1.009
	$|67\rangle$	0.000	0.000	3.037860	0.000	0.000	2.000	1.054	1.084
	$|66\rangle$	-0.011	-1.021	3.037810	0.000	0.000	1.000	0.527	0.542
	$|65\rangle$	0.000	0.000	3.037750	0.000	0.000	0.000	0.000	0.000
	$|64\rangle$	1.066	0.045	3.037700	0.000	0.000	-1.000	-0.527	-0.542
	$|63\rangle$	0.000	0.000	3.037640	0.000	0.000	-2.000	-1.054	-1.084
	$|62\rangle$	-1.066	-0.045	3.024640	0.000	0.000	1.000	0.580	0.592
	$|61\rangle$	0.000	0.000	3.024580	0.000	0.000	0.000	0.000	0.000
	$|60\rangle$	0.026	0.992	3.024530	0.000	0.000	-1.000	-0.580	-0.592
	$|59\rangle$	0.000	0.000	3.019140	0.000	0.000	0.000	0.000	0.000
	$|58\rangle$	-0.026	-0.992	2.899320	0.000	0.000	1.000	0.312	0.074
	$|57\rangle$	0.000	0.000	2.899270	0.000	0.000	0.000	0.000	0.000
	$|56\rangle$	1.067	0.013	2.899220	0.000	0.000	-1.000	-0.312	-0.074

3

$\|55\rangle$	0.000	0.000	2.568280	0.000 0.000 0.000 0.000			0.000
$\|54\rangle$	-1.067	-0.013	2.517180	0.000 0.000 0.992 0.455			0.010
$\|53\rangle$	0.000	0.000	2.517130	0.000 0.000 0.000 0.000			0.000
$\|52\rangle$	1.074	0.002	2.517070	0.000 0.000 -0.992 -0.455			-0.010
$\|51\rangle$	0.000	0.000	2.442500	0.000 0.000 0.831 0.844			0.002
$\|50\rangle$	-1.074	-0.002	2.442400	0.000 0.000 0.000 0.000			0.000
$\|49\rangle$	0.000	0.000	2.442370	0.000 0.000 -0.831 -0.844			-0.002
$\|48\rangle$	0.001	1.030	2.434180	0.000 0.000 0.993 0.006			1.042
$\|47\rangle$	0.000	0.000	2.434110	0.000 0.000 0.000 0.000			0.000
$\|46\rangle$	-0.001	-1.030	2.434070	0.000 0.000 -0.992 -0.006			-1.042
$\|45\rangle$	0.069	0.569	2.423920	0.000 0.000 0.000 0.000			0.000
$\|44\rangle$	0.000	0.000	2.396940	0.000 0.000 0.000 0.000			0.000
$\|43\rangle$	-0.069	-0.569	2.396520	0.000 0.000 0.999 0.011			1.020
$\|42\rangle$	0.000	0.000	2.396470	0.000 0.000 0.000 0.000			0.000
$\|41\rangle$	0.992	0.062	2.396420	0.000 0.000 -1.000 -0.011			-1.020
$\|40\rangle$	0.000	0.000	2.338180	0.000 0.000 0.000 0.000			0.000
$\|39\rangle$	-0.992	-0.062	2.278280	0.000 0.000 1.000 1.066			0.045
$\|38\rangle$	0.312	0.074	2.278220	0.000 0.000 0.000 0.000			0.000
$\|37\rangle$	0.000	0.000	2.278170	0.000 0.000 -1.000 -1.066			-0.045
$\|36\rangle$	-0.312	-0.074	2.021190	0.000 0.000 1.000 0.071			0.021
$\|35\rangle$	-0.013	1.009	2.021140	0.000 0.000 0.000 0.000			0.000
$\|34\rangle$	0.000	0.000	2.021090	0.000 0.000 -1.000 -0.071			-0.021
$\|33\rangle$	0.013	-1.009	1.665760	0.000 0.000 0.000 0.000			0.000
$\|32\rangle$	1.054	1.084	1.650800	0.000 0.000 0.000 0.000			0.000
$\|31\rangle$	0.527	0.542	1.648310	0.000 0.000 0.989 0.027			0.981
$\|30\rangle$	0.000	0.000	1.648260	0.000 0.000 0.000 0.000			0.000
$\|29\rangle$	-0.527	-0.542	1.648200	0.000 0.000 -0.989 -0.027			-0.982
$\|28\rangle$	-1.054	-1.084	1.638380	0.000 0.000 0.999 1.012			0.041
$\|27\rangle$	0.580	0.592	1.638330	0.000 0.000 0.000 0.000			0.000
$\|26\rangle$	0.000	0.000	1.638280	0.000 0.000 -0.999 -1.012			-0.041
$\|25\rangle$	-0.580	-0.592	1.576410	0.000 0.000 0.000 0.000			0.000
$\|24\rangle$	0.000	0.000	1.537190	0.000 0.000 0.996 1.063			0.013

$\lvert 23\rangle$	0.459	0.010	1.537130	0.000	0.000	0.000	0.000	0.000
$\lvert 22\rangle$	0.000	0.000	1.537080	0.000	0.000	-0.996	-1.063	-0.013
$\lvert 21\rangle$	-0.459	-0.010	1.534630	0.000	0.000	0.000	-0.001	0.000
$\lvert 20\rangle$	0.071	0.021	1.310590	0.000	0.000	1.000	-0.196	0.998
$\lvert 19\rangle$	0.000	0.000	1.310540	0.000	0.000	0.000	0.000	0.000
$\lvert 18\rangle$	-0.071	-0.021	1.310480	0.000	0.000	-1.000	0.195	-0.998
$\lvert 17\rangle$	0.000	0.000	1.299560	0.000	0.000	2.000	1.057	1.043
$\lvert 16\rangle$	1.013	0.041	1.299510	0.000	0.000	1.000	0.528	0.522
$\lvert 15\rangle$	0.000	0.000	1.299450	0.000	0.000	0.000	0.000	0.000
$\lvert 14\rangle$	-1.013	-0.041	1.299400	0.000	0.000	-1.000	-0.528	-0.522
$\lvert 13\rangle$	-0.195	0.998	1.299340	0.000	0.000	-2.000	-1.057	-1.043
$\lvert 12\rangle$	0.000	0.000	1.295390	0.000	0.000	1.000	0.676	0.657
$\lvert 11\rangle$	0.195	-0.998	1.295340	0.000	0.000	0.000	0.000	0.000
$\lvert 10\rangle$	1.057	1.043	1.295280	0.000	0.000	-1.000	-0.675	-0.657
$\lvert 9\rangle$	0.528	0.522	1.293980	0.000	0.000	0.000	0.000	0.000
$\lvert 8\rangle$	0.000	0.000	0.162670	0.000	0.000	0.000	0.000	0.000
$\lvert 7\rangle$	-0.528	-0.522	0.149710	0.000	0.000	1.000	1.074	0.002
$\lvert 6\rangle$	-1.057	-1.043	0.149660	0.000	0.000	0.000	0.000	0.000
$\lvert 5\rangle$	0.675	0.657	0.149600	0.000	0.000	-1.000	-1.074	-0.002
$\lvert 4\rangle$	0.000	0.000	0.104640	0.000	0.000	0.000	0.000	0.000
$\lvert 3\rangle$	-0.675	-0.657	0.000110	0.000	0.000	1.000	0.001	1.030
$\lvert 2\rangle$	0.000	0.000	0.000050	0.000	0.000	0.000	0.000	0.000
$\lvert 1\rangle$	-0.002	0.000	0.000000	0.000	0.000	-1.000	-0.001	-1.030

Also, Table II shows the spin density, energies, and expectation values of the spin angular momentum elements for the spin-flip and spin-transfer scenarios on non-linear zigzag carbon chain structure $Ni_2@C_{36}H_{36}$ for the appropriate many-body states before and after inclusion spin-orbit-coupling and the magnetic field.

TABLE II: Spin density, energies, and expectation values of the spin angular momentum elements for the spin-flip and spin-transfer scenarios on non-linear zigzag carbon chain structure $Ni_2@C_{36}H_{36}$ for the appropriate many-body states before and after inclusion spin-orbit-coupling and the magnetic field. The sign of $\langle S_x \rangle$, $\langle S_y \rangle$, and $\langle S_z \rangle$ signifies the spin direction: the positive and negative values are spin-up $\alpha \uparrow$ and spin-down $\beta \downarrow$, respectively.

| Method | States | Spin density before SOC and B | | Energy, spins directions and spin density after SOC and B | | | | | |
		Ni1	Ni2	E (eV)	$\langle S_x \rangle$	$\langle S_y \rangle$	$\langle S_z \rangle$	Ni1	Ni2
EOM-CCSD	$\lvert 71 \rangle$	0.000	0.000	3.253340	0.000	0.000	0.000	0.000	0.000
	$\lvert 70 \rangle$	0.000	0.000	3.243930	0.000	0.000	1.000	0.993	0.060
	$\lvert 69 \rangle$	-0.660	-0.668	3.243870	0.000	0.000	0.000	0.000	0.000
	$\lvert 68 \rangle$	0.000	0.000	3.243820	0.000	0.000	-1.000	-0.993	-0.060
	$\lvert 67 \rangle$	0.660	0.668	3.121150	0.000	0.000	1.000	-0.029	0.999
	$\lvert 66 \rangle$	-1.045	-1.058	3.121100	0.000	0.000	0.000	0.000	0.000
	$\lvert 65 \rangle$	-0.522	-0.529	3.121040	0.000	0.000	-1.000	0.029	-0.999
	$\lvert 64 \rangle$	0.000	0.000	3.105210	0.000	0.000	2.000	1.045	1.047
	$\lvert 63 \rangle$	0.522	0.529	3.105150	0.000	0.000	1.000	0.523	0.524
	$\lvert 62 \rangle$	1.045	1.058	3.105100	0.000	0.000	0.000	0.000	0.000
	$\lvert 61 \rangle$	-0.951	0.120	3.105040	0.000	0.000	-1.000	-0.523	-0.524
	$\lvert 60 \rangle$	0.000	0.000	3.104990	0.000	0.000	-2.000	-1.045	-1.047
	$\lvert 59 \rangle$	0.951	-0.120	3.103170	0.000	0.000	1.000	0.579	0.590
	$\lvert 58 \rangle$	-0.022	-0.969	3.103120	0.000	0.000	0.000	0.000	0.000
	$\lvert 57 \rangle$	0.000	0.000	3.103060	0.000	0.000	-1.000	-0.579	-0.590
	$\lvert 56 \rangle$	0.022	0.969	3.102310	0.000	0.000	0.000	0.000	0.000
	$\lvert 55 \rangle$	0.000	0.000	2.720890	0.000	0.000	1.000	0.446	0.189
	$\lvert 54 \rangle$	-0.023	-0.118	2.720830	0.000	0.000	0.000	0.000	0.000
	$\lvert 53 \rangle$	0.000	0.000	2.720780	0.000	0.000	-1.000	-0.446	-0.189
	$\lvert 52 \rangle$	0.023	0.118	2.435800	0.000	0.000	1.000	1.065	0.001
	$\lvert 51 \rangle$	-0.446	-0.189	2.435750	0.000	0.000	0.000	0.000	0.000
	$\lvert 50 \rangle$	0.000	0.000	2.435690	0.000	0.000	-1.000	-1.065	-0.001
	$\lvert 49 \rangle$	0.446	0.189	2.427530	0.000	0.000	0.000	0.000	0.000
	$\lvert 48 \rangle$	-1.045	-1.047	2.373440	0.000	0.000	0.998	0.000	1.002
	$\lvert 47 \rangle$	-0.523	-0.524	2.373380	0.000	0.000	0.000	0.000	0.000

$\lvert 46\rangle$	0.000	0.000	2.373330	0.000	0.000	-0.998	0.000	-1.002
$\lvert 45\rangle$	0.523	0.524	2.357990	0.000	0.000	0.000	0.000	0.000
$\lvert 44\rangle$	1.045	1.047	2.129480	0.000	0.000	0.000	0.000	0.000
$\lvert 43\rangle$	-0.579	-0.590	2.089280	0.000	0.000	1.000	0.004	1.052
$\lvert 42\rangle$	0.000	0.000	2.089220	0.000	0.000	0.000	0.000	0.000
$\lvert 41\rangle$	0.579	0.590	2.089170	0.000	0.000	-1.000	-0.004	-1.052
$\lvert 40\rangle$	0.000	0.000	2.064380	0.000	0.000	1.000	0.023	0.118
$\lvert 39\rangle$	0.029	-0.998	2.064320	0.000	0.000	0.000	0.000	0.000
$\lvert 38\rangle$	0.000	0.000	2.064270	0.000	0.000	-1.000	-0.023	-0.118
$\lvert 37\rangle$	-0.029	0.998	2.002910	0.000	0.000	0.000	0.000	0.000
$\lvert 36\rangle$	0.000	0.000	1.988790	0.000	0.000	1.000	1.045	0.002
$\lvert 35\rangle$	-0.993	-0.060	1.988730	0.000	0.000	0.000	0.000	0.000
$\lvert 34\rangle$	0.000	0.000	1.988680	0.000	0.000	-1.000	-1.045	-0.002
$\lvert 33\rangle$	0.993	0.060	1.570390	0.000	0.000	0.000	0.000	0.000
$\lvert 32\rangle$	-1.019	0.000	1.530030	0.000	0.000	0.978	0.002	1.048
$\lvert 31\rangle$	0.000	0.000	1.529960	0.000	0.000	0.000	0.000	0.000
$\lvert 30\rangle$	1.019	0.000	1.529920	0.000	0.000	-0.978	-0.002	-1.048
$\lvert 29\rangle$	0.000	0.000	1.503830	0.000	0.000	0.000	0.000	0.000
$\lvert 28\rangle$	0.000	0.000	1.427060	0.000	0.000	0.000	0.000	0.000
$\lvert 27\rangle$	0.000	-1.072	1.423610	0.000	0.000	1.000	1.034	0.006
$\lvert 26\rangle$	0.000	0.000	1.423560	0.000	0.000	0.000	0.000	0.000
$\lvert 25\rangle$	0.000	1.072	1.423500	0.000	0.000	-1.000	-1.034	-0.006
$\lvert 24\rangle$	-1.033	-0.006	1.335560	0.000	0.000	0.000	0.000	0.000
$\lvert 23\rangle$	0.000	0.000	1.323440	0.000	0.000	1.000	0.025	0.966
$\lvert 22\rangle$	1.033	0.006	1.323370	0.000	0.000	0.000	0.000	0.000
$\lvert 21\rangle$	0.000	0.000	1.323330	0.000	0.000	-1.000	-0.024	-0.966
$\lvert 20\rangle$	-0.002	-1.071	1.319520	0.000	0.000	1.000	0.949	-0.117
$\lvert 19\rangle$	0.000	0.000	1.319480	0.000	0.000	0.000	0.000	0.000
$\lvert 18\rangle$	0.002	1.071	1.319410	0.000	0.000	-1.000	-0.949	0.117
$\lvert 17\rangle$	0.000	0.000	1.308150	0.000	0.000	2.000	1.045	1.058
$\lvert 16\rangle$	-1.044	-0.002	1.308090	0.000	0.000	1.000	0.523	0.529
$\lvert 15\rangle$	0.000	0.000	1.308030	0.000	0.000	0.000	0.000	0.000

$|14\rangle$	1.044	0.002	1.307980	0.000	0.000	-1.000	-0.523	-0.529
$|13\rangle$	0.000	0.000	1.307930	0.000	0.000	-2.000	-1.045	-1.058
$|12\rangle$	-0.004	-1.052	1.306080	0.000	0.000	1.000	0.659	0.669
$|11\rangle$	0.000	0.000	1.306020	0.000	0.000	0.000	0.000	0.000
$|10\rangle$	0.004	1.052	1.305970	0.000	0.000	-1.000	-0.659	-0.669
$|9\rangle$	0.000	0.000	1.305280	0.000	0.000	0.000	0.000	0.000
$|8\rangle$	-1.065	-0.001	0.089390	0.000	0.000	1.000	0.000	1.072
$|7\rangle$	0.000	0.000	0.089340	0.000	0.000	0.000	0.000	0.000
$|6\rangle$	1.065	0.001	0.089280	0.000	0.000	-1.000	0.000	-1.072
$|5\rangle$	0.000	0.000	0.045350	0.000	0.000	0.000	0.000	0.000
$|4\rangle$	0.000	-1.004	0.032570	0.000	0.000	1.000	1.019	0.000
$|3\rangle$	0.000	0.000	0.032520	0.000	0.000	0.000	0.000	0.000
$|2\rangle$	0.000	1.004	0.032470	0.000	0.000	-1.000	-1.019	0.000
$|1\rangle$	0.000	0.000	0.000000	0.000	0.000	0.000	0.000	0.000

Since the spin density distribution fulfills the requirements to accomplish the spin dynamics processes on $Ni_2@C_{32}H_{32}$ and $Ni_2@C_{36}H_{36}$. Therefore, several spin-transfer scenarios are achieved. We present some of them in Fig. 2 ($Ni_2@C_{32}H_{32}$) and in Fig. 3 ($Ni_2@C_{36}H_{36}$). Besides, the optimized parameters of the laser pulses are shown in Table III.

Moreover, the reserved spin-transfer processes with the same laser pulses on $Ni_2@C_{32}H_{32}$ and $Ni_2@C_{36}H_{362}$ are accomplished and shown in Figs. 4-5, respectively. Their optimized parameters of the laser pulses are given in Table IV.

FIG. 2. Spin-transfer processes on $Ni_2@C_{32}H_{32}$: Ni2→Ni1 ($|3\rangle \to |7\rangle$), Ni1→Ni2 ($|7\rangle \to |31\rangle$), Ni1→Ni2 ($|37\rangle \to |46\rangle$), Ni1→Ni2 ($|39\rangle \to |43\rangle$), Ni1→Ni2 ($|39\rangle \to |48\rangle$), and Ni2→Ni1 ($|41\rangle \to |49\rangle$). The time-dependent population of the initial (dashed black line), final or target (solid red line), and intermediate (solid lines in different colors) states.
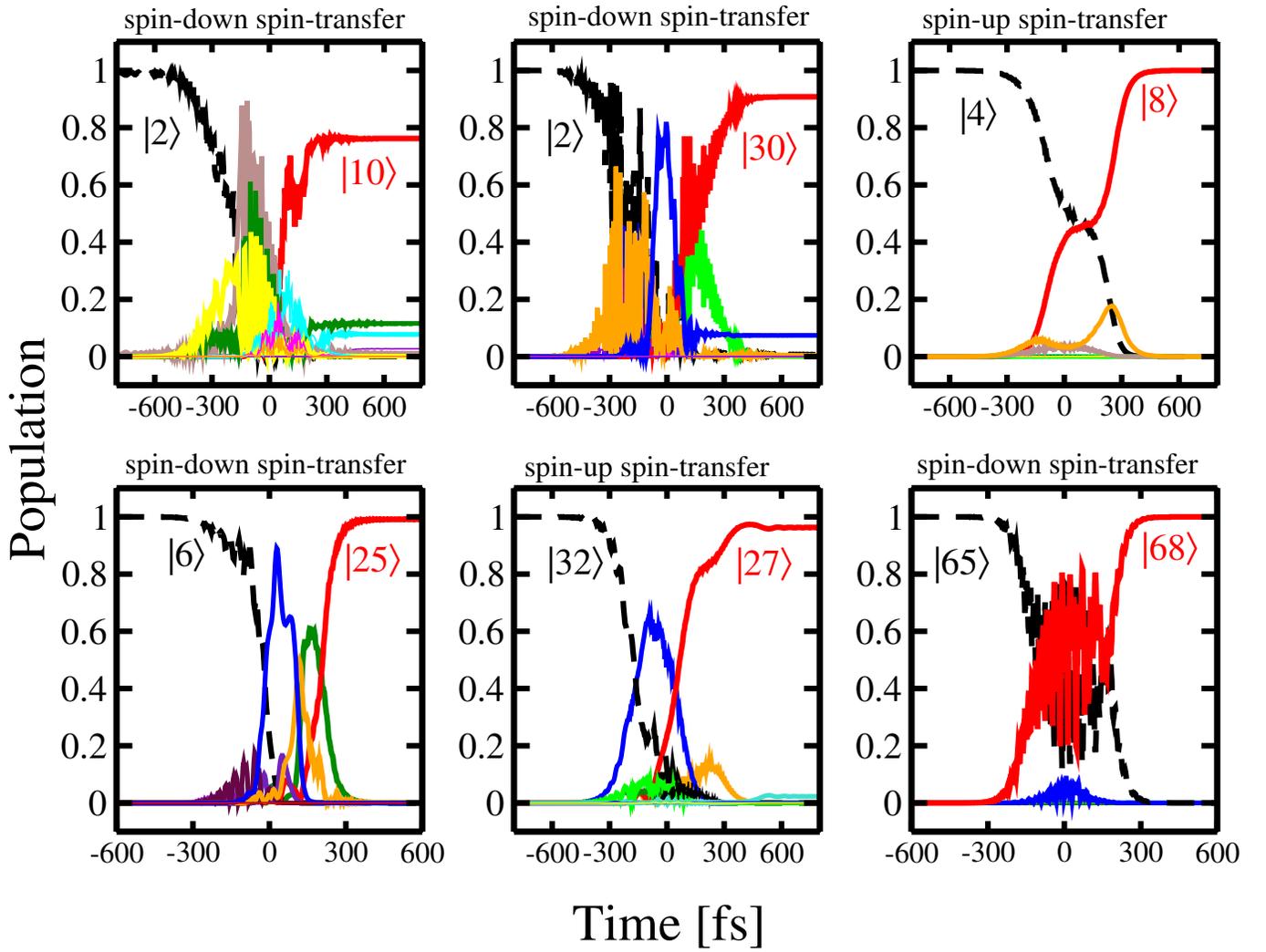
FIG. 3. Spin-transfer processes on $Ni_2@C_{36}H_{36}$: Ni1→Ni2 ($|2\rangle \to |10\rangle$), Ni1→Ni2 ($|2\rangle \to |30\rangle$), Ni1→Ni2 ($|4\rangle \to |8\rangle$), Ni2→Ni1 ($|6\rangle \to |25\rangle$), Ni2→Ni2 ($|32\rangle \to |27\rangle$), and Ni2→Ni1 ($|65\rangle \to |68\rangle$). The time-dependent population of the initial (dashed black line), final or target (solid red line), and intermediate (solid lines in different colors) states.

10

TABLE III. Spin localized, possible scenarios and the parameters of the laser pulses are optimized with our own genetic algorithm program and EOM-CCSD method: ΔE is the energy difference between the initial and last (target) states, the angles of incidence in spherical coordinates θ (°), and ϕ (°), the angle between the polarization of light and the optical plane γ (°), the full width at half-maximum of the laser pulse (FWHM), the laser energy E_{laser}, the amplitude of the laser pulse, and the chirp, which indicates the linear sweep of the frequency with respect to the peak frequency. The ranges of θ (°) and ϕ (°) are from [0°, 180°] and [0°, 360°], respectively. Also, the range of γ is from [0°, 360°] for both structures $Ni_2@C_{32}H_{32}$ and $Ni_2@C_{32}H_{36}$.

System	Method	Scenario	Spin localized	Process	Fidelity (%)[a]	ΔE (eV)	θ (°)	ϕ (°)	γ (°)	FWHM (fs)	E_{laser} (eV)	chirp
$Ni_2@C_{32}H_{32}$	EOM-CCSD	spin-transfer	Ni2 → Ni1	$\lvert3\uparrow\rangle \to \lvert7\uparrow\rangle$	99.97	0.1960	283.94	120.80	221.48	317.37	3.164	0.985
		spin-transfer	Ni1 → Ni2	$\lvert7\uparrow\rangle \to \lvert31\uparrow\rangle$	97.45	1.4986	288.76	15.99	326.95	489.64	1.545	0.991
		spin-transfer	Ni1 → Ni2	$\lvert37\downarrow\rangle \to \lvert46\downarrow\rangle$	96.377	0.1559	268.064	290.73	275.68	282.20	2.782	1.023
		spin-transfer	Ni1 → Ni2	$\lvert39\uparrow\rangle \to \lvert43\uparrow\rangle$	99.92	0.11824	90.12	135.09	133.62	382.70	2.098	1.010
		spin-transfer	Ni1 → Ni2	$\lvert39\uparrow\rangle \to \lvert48\uparrow\rangle$	99.16	0.1559	276.39	340.64	263.21	376.53	3.039	1.029
		spin-transfer	Ni2 → Ni1	$\lvert41\downarrow\rangle \to \lvert49\downarrow\rangle$	99.92	0.04595	251.16	305.79	306.79	320.43	2.471	1.028
$Ni_2@C_{36}H_{36}$	EOM-CCSD	spin-transfer	Ni2 → Ni1	$\lvert2\downarrow\rangle \to \lvert10\downarrow\rangle$	76.22	1.2735	96.14	245.30	353.31	402.24	2.303	1.049
		spin-transfer	Ni1 → Ni2	$\lvert2\downarrow\rangle \to \lvert30\downarrow\rangle$	90.78	1.49745	84.51	296.98	50.57	370.68	1.668	1.041
		spin-transfer	Ni1 → Ni2	$\lvert4\uparrow\rangle \to \lvert8\uparrow\rangle$	100	0.05682	264.62	253.28	3.22	481.43	2.752	0.978
		spin-transfer	Ni2 → Ni1	$\lvert6\downarrow\rangle \to \lvert25\downarrow\rangle$	99.15	1.33422	302.33	243.18	186.58	287.78	1.375	1.023
		spin-transfer	Ni2 → Ni1	$\lvert32\uparrow\rangle \to \lvert27\uparrow\rangle$	96.26	0.10642	271.88	2.985	29.87	406.74	1.471	0.9728
		spin-transfer	Ni2 → Ni1	$\lvert65\downarrow\rangle \to \lvert68\downarrow\rangle$	99.97	0.12278	162.11	326.60	312.63	241.97	0.133	0.950

[a] fidelity is defined as the population of the goal state following the influence of the laser pulse.

TABLE IV. Spin localized, reversed possible spin-transfer scenarios and the parameters of the laser pulses are optimized with our own genetic algorithm program and EOM-CCSD method for both structures $Ni_2@C_{32}H_{32}$ and $Ni_2@C_{32}H_{36}$.

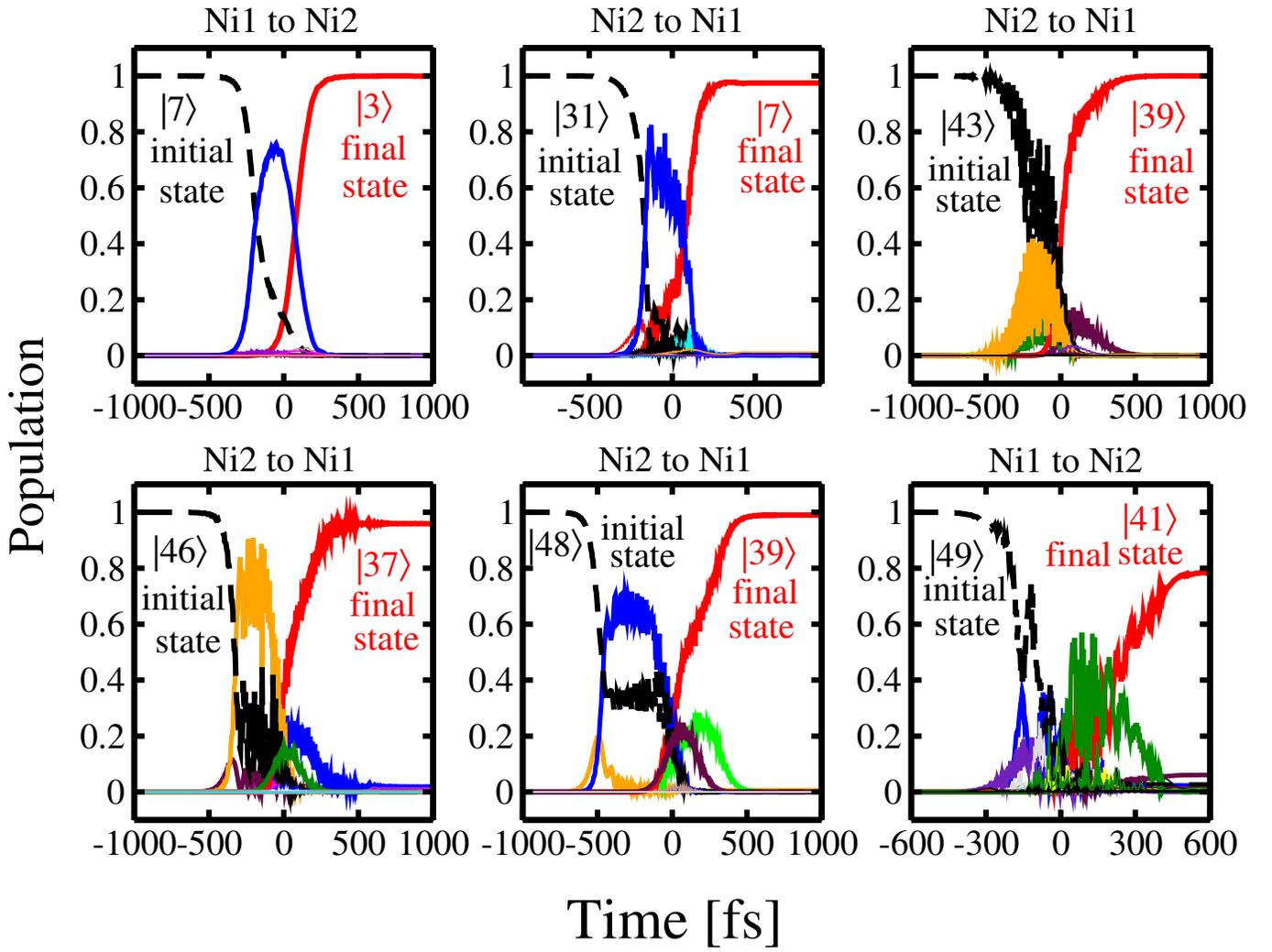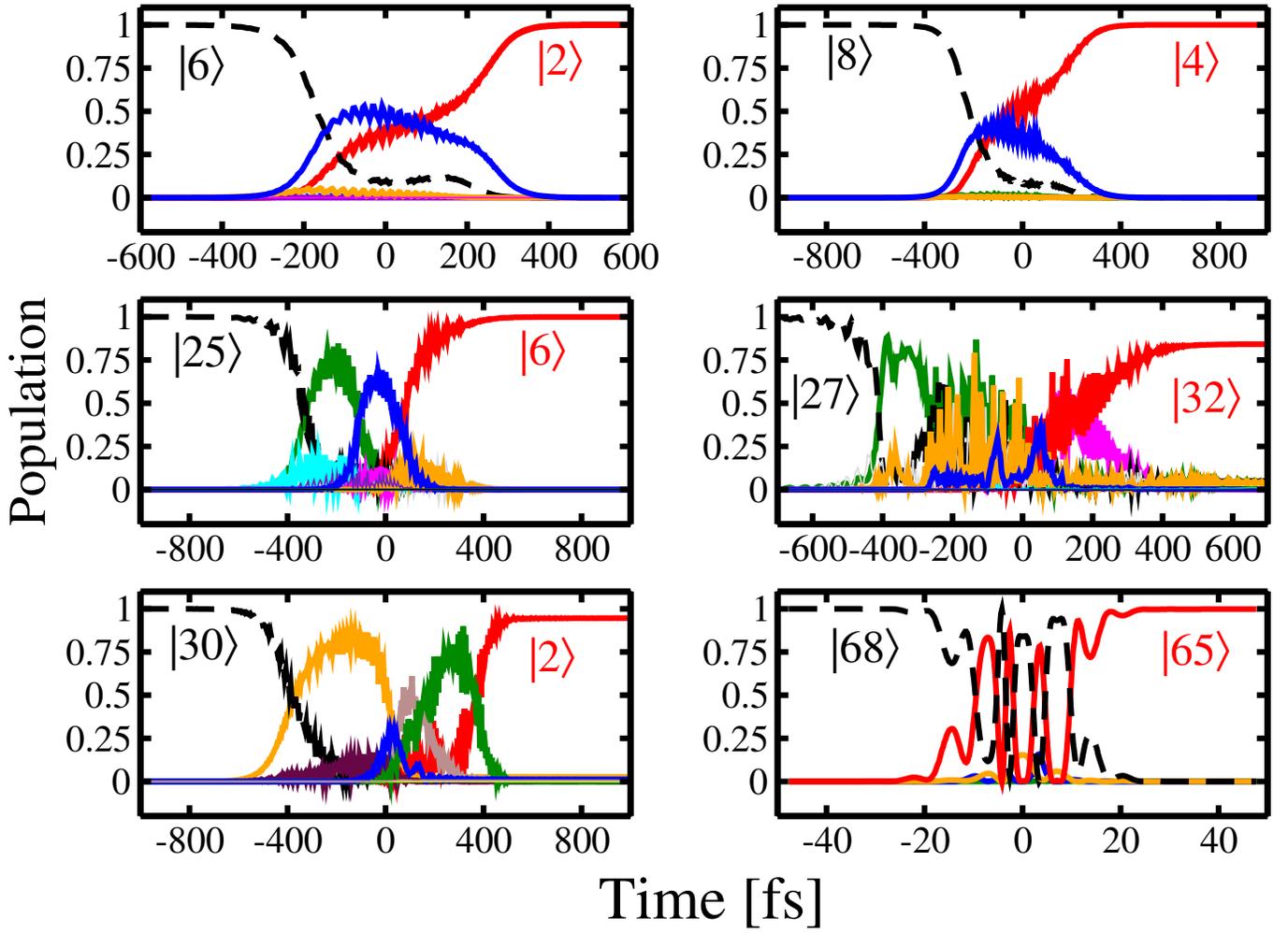| System	Method	Scenario	Spin localized	Process	Fidelity (%)	ΔE (eV)	θ (°)	ϕ (°)	γ (°)	FWHM (fs)	E_{laser} (eV)	chirp
$Ni_2@C_{32}H_{32}$	EOM-CCSD	spin-transfer	Ni1 → Ni2	$\lvert7\uparrow\rangle \to \lvert3\uparrow\rangle$	99.90	0.1960	88.60	320.68	329.90	430.49	2.825	1.017
		spin-transfer	Ni2 → Ni1	$\lvert31\uparrow\rangle \to \lvert7\uparrow\rangle$	97.54	1.4986	89.52	194.77	109.35	359.08	1.551	1.010
		spin-transfer	Ni2 → Ni1	$\lvert46\downarrow\rangle \to \lvert37\downarrow\rangle$	95.94	0.1559	259.31	5.13	27.30	451.80	2.177	0.9502
		spin-transfer	Ni2 → Ni1	$\lvert43\uparrow\rangle \to \lvert39\uparrow\rangle$	100	0.11824	84.31	295.82	32.71	493.59	1.815	0.995
		spin-transfer	Ni2 → Ni1	$\lvert48\uparrow\rangle \to \lvert39\uparrow\rangle$	98.98	0.1559	113.88	78.76	303.19	451.80	2.176	0.971
		spin-transfer	Ni1 → Ni2	$\lvert49\downarrow\rangle \to \lvert41\downarrow\rangle$	78.43	0.04595	55.35	33.40	125.81	294.67	0.752	0.990
$Ni_2@C_{36}H_{36}$	EOM-CCSD	spin-transfer	Ni2 → Ni1	$\lvert6\downarrow\rangle \to \lvert2\downarrow\rangle$	100	0.05681	105.71	315.66	186.87	338.02	2.634	1.010
		spin-transfer	Ni2 → Ni1	$\lvert8\uparrow\rangle \to \lvert4\uparrow\rangle$	100	0.05682	93.95	145.09	181.08	402.66	2.689	1.013
		spin-transfer	Ni1 → Ni2	$\lvert27\uparrow\rangle \to \lvert32\uparrow\rangle$	84.12	0.10642	231.17	288.90	1.35	382.16	1.724	1.020
		spin-transfer	Ni2 → Ni1	$\lvert30\downarrow\rangle \to \lvert2\downarrow\rangle$	94.55	1.49745	114.76	21.48	17.64	484.72	1.359	0.9715
		spin-transfer	Ni1 → Ni2	$\lvert25\downarrow\rangle \to \lvert6\downarrow\rangle$	99.93	1.33422	96.10	218.30	16.93	493.89	1.398	0.966
		spin-transfer	Ni1 → Ni2	$\lvert68\downarrow\rangle \to \lvert65\downarrow\rangle$	99.75	0.12278	198.70	235.93	301.14	19.06	0.293	1.020

FIG. 4. The reserved spin-transfer processes with the same laser pulses on $Ni_2@C_{32}H_{32}$: Ni1→Ni2 ($|7\rangle \to |3\rangle$), Ni2→Ni1 ($|31\rangle \to |7\rangle$), Ni2→Ni1 ($|43\rangle \to |39\rangle$), Ni2→Ni1 ($|46\rangle \to |39\rangle$), Ni2→Ni1 ($|48\rangle \to |39\rangle$), and Ni1→Ni2 ($|49\rangle \to |41\rangle$). The time-dependent population of the initial (dashed black line), final or target (solid red line), and intermediate (solid lines in different colors) states.

FIG. 5. The reserved spin-transfer processes with the same laser pulses on Ni$_2$@C$_{36}$H$_{36}$: Ni2→Ni1 ($|6\rangle \to |2\rangle$), Ni2→Ni1 ($|8\rangle \to |4\rangle$), Ni1→Ni2 ($|25\rangle \to |6\rangle$), Ni1→Ni2 ($|27\rangle \to |32\rangle$), Ni2→Ni1 ($|30\rangle \to |2\rangle$), and Ni1→Ni2 ($|68\rangle \to |65\rangle$). The time-dependent population of the initial (dashed black line), final or target (solid red line), and intermediate (solid lines in different colors) states.